13.8 A NUMERICAL STUDY OF THE EFFECTS OF AMBIENT WIND DIRECTION ON FLOW AND DISPERSION IN URBAN STREET CANYONS USING THE RNG k-ε TURBULENCE MODEL

Jae-Jim Kim* and Jong-Jin Baik
Seoul National University, Seoul, Korea

1. INTRODUCTION

Numerical models are very useful tools not only to do risk assessment of hazardous materials emitted to the atmosphere in urban areas but also to give us desirable guidelines for optimizing ventilation, ensuring sunshine, and reducing heat island effects in urban areas. Various types of numerical models have been used to simulate urban flow and dispersion. Turbulence modeling is necessary in using Reynolds-averaged Navier-Stokes equations (RANS) models. The standard k-ε turbulence model that is most commonly used has deficiencies when it is applied to the simulation of flow impingement and separation (Castro and Apsley 1997). Another variant of the standard k-ε turbulence model is the renormalization group (RNG) k-ε turbulence model. The main idea of the RNG method is to systematically remove small scales of turbulence by expressing their effects in terms of larger scale motions and a modified viscosity (Yakhot et al. 1992).

The main objectives of this study are to develop a three-dimensional computational fluid dynamics (CFD) model with the RNG k-ε turbulence scheme and to investigate the effects of inflow wind direction on flow and dispersion in urban areas using the developed model.

2. MODEL DESCRIPTION

The governing equations used in this numerical model are the same as those in Baik et al. (2003) except for the prognostic equation for the dissipation rate of turbulent kinetic energy (TKE) and turbulent viscosity (K_m). In the present CFD model, the RNG k-ε turbulence scheme established by Yakhot et al. (1992) is used. This scheme differs from a standard k-ε turbulence scheme in that it includes an additional sink term in the turbulence dissipation equation to account for non-equilibrium strain rates and employs different values for the model coefficients.

In modeling urban flow and dispersion, smaller grid sizes are desirable near buildings to better resolve flow and dispersion fields there, but away from buildings larger grid sizes are allowable. To make the CFD model efficient for a given computing resource, a non-uniform grid system is implemented in the model, following Versteeg and Malalasekera (1995). The governing equation set is numerically solved on a staggered grid system using a finite volume method with the semi-implicit method for pressure-linked equation (SIMPLE) algorithm (Patankar 1980). For further details of the numerical procedure, see Baik et al. (2003).

3. EXPERIMENTAL SETUP

To study the effects of ambient wind direction on flow and pollutant dispersion in urban areas, a group of buildings are considered and a non-uniform grid system with 101 cells in the x- and y-directions and 41 cells in the z-direction is used (Fig. 1). The dimension of the smallest cell is 0.3 m × 0.3 m × 0.3 m in the x-, y-, and z-directions, which is situated at the edges of the buildings. The expansion ratio in the present non-uniform grid system is 1.1. The largest cell dimension is 1.8 m × 1.8 m × 1.8 m. Castro and Apsley (1997) used an expansion ratio of 1.07 and Zhang et al. (1996) used expansion ratios not exceeding 1.3. The computational domain size is 63.1 m × 63.1 m × 28.5 m in the x-, y-, and z-directions, respectively. Four buildings located around the center of the domain are cubic. The street width (W) between the buildings is the same as the building length (L) and the building height (H). So, the street aspect ratios, H/W and L/W, are all equal to 1. For convenience, the street canyons between the buildings I and II, II and III, III and IV, and IV and I (Fig. 1) are called west, south, east, and north street canyons, respectively. The time step used is 0.05 s. For better resolving small-scale fluctuations in time, a relatively small time step is used. The numerical model is integrated up to t = 20 min. An investigation of time dependency indicated that a quasi-steady state in the flow field is established after t = 5 ~ 7 min. Passive pollutants are continuously released from the centers of the first cells above the ground surface (z = 0.15 m) between the four buildings starting from t = 10 min. It is assumed that pollutants released are homogeneously distributed in the source cells and that pollutants are released with an emission rate of 10 ppb s^{-1} at each source cell.

At the outflow and upper boundaries, zero-gradient condition is applied. At the solid surface, wall boundary conditions are applied, following Versteeg and Malalasekera (1995)

4. RESULTS AND DISCUSSION

a. Flow characteristics

Ten cases with different ambient wind directions are simulated and analyzed. The ambient wind direction (θ) varies from 0° to 45° with an increment

* Corresponding author address: Jae-Jin Kim, Seoul National University, Climate Environment System Research Center, Seoul, Korea 151-742; e-mail: jjkim@climate.snu.ac.kr

of 5°. Notice that if the ambient wind direction has an angle of $0° < \theta \le 45°$, the west and south edges of the computational domain are inflow boundaries. According to the ambient wind direction, simulated flows can be classified into three patterns in a view of the characteristics of the mean flow circulation generated behind the upwind building. The schematic of each flow pattern is presented in Fig. 2, which is drawn based on simulated flow analysis.

Flow pattern I: The first flow pattern appears when the ambient wind direction is perpendicular to the buildings ($\theta = 0°$). In this case, flow is symmetric about the center of the street canyon. Near the upwind building, flow is upward and outward. Near the downwind building, flow is downward and inward in the upper region, but it is downward and outward in the lower region. Near the street bottom, flow is predominantly outward. Behind the upwind building, there exists a portal vortex (Becker et al. 2002) whose ends are located near the lower edges of the downwind building. The portal vortex is symmetric about the center of the street canyon and its horizontal axis is perpendicular to the ambient wind direction. Flow coming into the street canyon curls up around the portal vortex. At the center of the street canyon, there is apparently no motion in the y-direction. The roll-type vortex rotating anticlockwise from the south view appears at the corner between the street bottom and the downwind building and it disappears near the center of the street canyon.

Flow pattern II: The second flow pattern appears when $5° \le \theta \le 20°$ (Fig. 2b). Similar to flow pattern I, a portal vortex is also generated. However, in flow pattern II, one footprint of the portal vortex is located near the street center and the other near the northeast edge of the upwind building. The difference in footprint position is associated with the wind direction near the street bottom. In flow pattern II, northeastward inflow from the canyon south is dominant near the southeast region of the street canyon. This causes the portal vortex to be detached from the downwind building. Near the north wall of the upwind building, an eddy circulation, which is absent in flow pattern I, is generated. The eddy circulation rotating clockwise is induced by flow separation. Incoming flow from the canyon south impinges on the building, producing stagnation point on the south and west walls of the downwind building and accordingly forming a horseshoe vortex around the building. The stagnation point due to flow impingement is also produced at the west and south walls of the upwind building.

Flow pattern III: This flow pattern occurs when $25° \le \theta \le 45°$. A portal vortex is also generated and its footprints are located behind the north and east walls of the upwind building (Fig. 2c). As the incident wind angle increases, the horizontal size of the portal vortex behind the east wall decreases, but that behind the north wall increases. As in flow pattern II, a horseshoe vortex is also generated along the south and west walls of the building. When the incident wind angle is 45°, flow is diagonally symmetric behind the upwind building. Above the building roof, recirculation zones are generated due to flow separation as flow impinges on the buildings. The y-z plane wind vector field at $x/H = 0.25$ shows a clockwise rotating vortex, which is evidence that the top of the portal vortex is slightly tilted towards the upwind region.

b. Dispersion characteristics

To examine the effects of ambient wind direction on scalar dispersion, pollutant sources are located close to the street bottom ($z = 0.15$ m, $z/H = 0.02$) in the east, west, south, and north street canyons and crossroad area between them. In this study, pollutant advection from the upwind region is not considered. Figure 8 shows pollutant concentration fields at $z = 1.6$ m (pedestrian level, $z/H = 0.17$) in the cases of $\theta = 0°$, 15°, and 45°. Pollutant concentration (in units of ppb) is presented on a logarithmic scale in base 10.

In the case of $\theta = 0°$ (Fig. 3a), very low concentration in the south (north) street canyon appears as going to the street-canyon center region from the downwind building because of inward and downward inflow having relatively low concentration. It is unexpected that in the south (north) street canyon pollutants are not trapped in the two vortices and the maximum concentration does not appear near the centers of the vortices. Concentration is relatively high near the upwind building and the south and north verges of the street canyon. Notice that the lowest concentration in the street canyon appears near the downwind building. Concentration in the west street canyon is very low. This means that most pollutants emitted are transported downwind before they are transported upward. There are high concentration bands beginning from the southeast and northeast edges of the upwind building. The bands extend downwind. Near the upwind building, pollutants transported to both sides of the street canyon by outward flow are transported upward by vertical motion and then escape from the street canyon. This explains why pollutants are not trapped in the vortices.

Unlike in the case of $\theta = 0°$, in the case of $\theta = 15°$ (Fig. 3b), the maximum concentration appears near the center of the larger vortex in the south (north) street canyon and concentration is relatively high around the larger vortex center. Low concentration appears in the west street canyon and the southeast region of the south street canyon. Concentration near the south wall of the building I is lower than in the case of $\theta = 0°$. Concentration in the downwind region is very low in the south street canyon but relatively high in the north street canyon. The fact that there is no emission source outside of the central four buildings gives an explanation for the difference. In the south street canyon, relatively clean air continuously comes into the street canyon from outside and it dilutes polluted air. On the other hand, in the north street canyon, the incoming air is already polluted by passing through the emission sources,

thus increasing concentration. The local maximum also appears near the northeast edge of the upwind building where the portal vortex exists. Pollutants are trapped along the north wall of the upwind building where flow is separated and eddy circulation is generated.

In the case of $\theta = 45°$ (Fig. 3c), concentration field is diagonally symmetric. Four high concentration regions appear around the centers of the vortices as pollutants emitted are trapped within the vortices. Concentration is very low in the southeast region of the south street canyon and in the northwest region of the west street canyon where relatively clean air arrives.

5. SUMMARY AND CONCLUSION

According to the ambient wind direction, three flow patterns could be classified in a view of the characteristics of the mean flow circulation generated behind the upwind building. In the first flow pattern, a portal vortex generated behind the east wall of the upwind building is symmetric about the center of the street canyon. Near the street bottom, outward flow is dominant, which makes the footprints of the portal vortex be located near the lower edges of the downwind building. Also, a roll-type standing vortex is generated at the corner between the street bottom and the downwind building. In the second flow pattern, a portal vortex is also generated behind the east wall of the upwind building. Its footprints are located near the center of the street canyon and the northeast edge of the upwind building. The horizontal size of the south-side portal vortex is larger than that of the north-side one. The portal vortex is slightly tilted anticlockwise in the horizontal. An eddy circulation is generated behind the north wall of the upwind building where flow separates. In the third flow pattern, a portal vortex is generated and its footprints are located behind the east and north walls of the upwind building. When the incident wind angle is 45°, flow is diagonally symmetric behind the upwind building. A horseshoe vortex is generated in front of the building. As the incident wind angle increases, pollutant escape from the street canyons decreases. Except for the case of $\theta = 0°$, pollutants are trapped in the portal vortex and high concentration appears there. When $\theta = 0°$, pollutants are transported to both side verges of the street canyon by outward flow dominant near the street bottom. Then, pollutants escape from the street canyon.

This study demonstrated that changes in ambient wind direction can make large differences in the mean flow circulation and accordingly the spatial distribution of passive pollutants. It is concluded that the ambient wind direction can greatly affect flow and dispersion around a group of buildings.

ACKNOWLEDGEMENTS

REFERENCES

Baik, J.-J., Kim, J.-J., Fernando, H. J. S., 2003. A CFD model for simulating urban flow and dispersion. Journal of Applied Meteorology 42, 1636-1648.

Becker, S., Lienhart, H., Durst, F., 2002. Flow around three-dimensional obstacles in boundary layers. Journal of Wind Engineering and Industrial Aerodynamics 90, 265-279.

Castro, I. P., Apsley, D. D., 1997. Flow and dispersion over topography: a comparison between numerical and laboratory data for two-dimensional flows. Atmospheric Environment 31, 839-850.

Patankar, S. V., 1980. Numerical Heat Transfer and Fluid Flow, pp. 126-131. McGraw-Hill, New York.

Versteeg, H. K., Malalasekera, W., 1995: An Introduction to Computational Fluid Dynamics: The Finite Volume Method, pp. 198-203 & 243-244. Longman, Malaysia.

Yakhot, V., Orszag, S. A., Thangam, S., Gatski, T. B., Speziale, C. G., 1992. Development of turbulence models for shear flows by a double expansion technique. Physics of Fluids A4, 1510-1520.

(a)

(b)
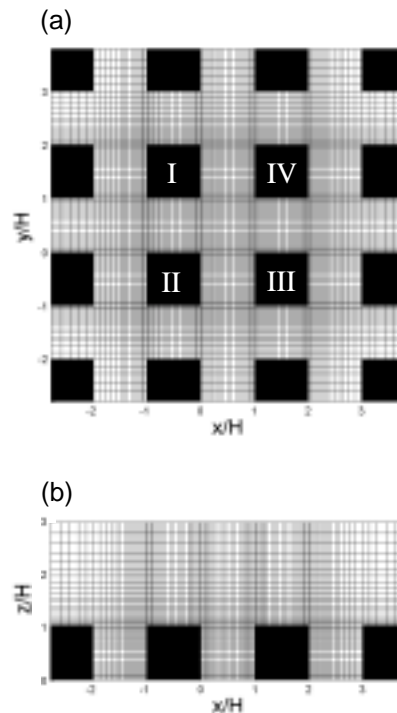
Figure 1. The (a) top view and (b) side view of the computational domain and grid system.

(a) flow pattern I

portal vortex

roll-type vortex

(b) flow pattern II

eddy circulation

horseshoe vortex

(c) flow pattern III

recirculation zone
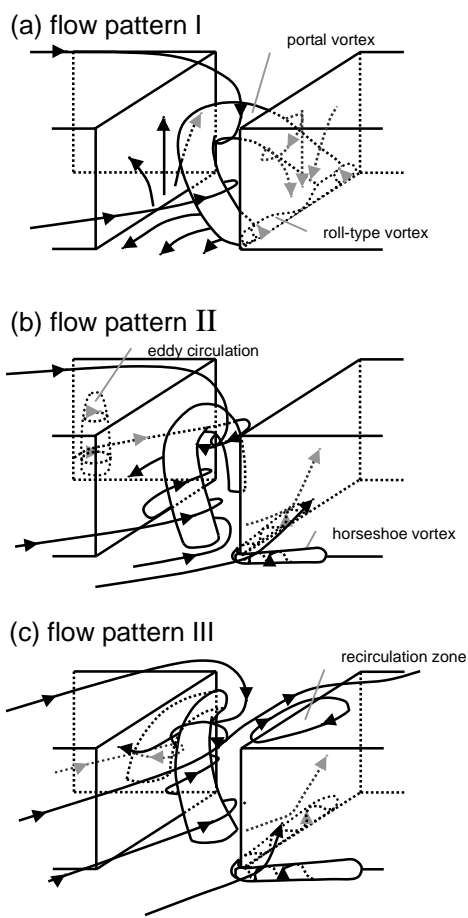
Figure 2. The schematic of the mean flow circulation according to different ambient wind directions. The dimensions of the portal vortex depicted here are reduced for the clarity of figure.

(b)

(c)
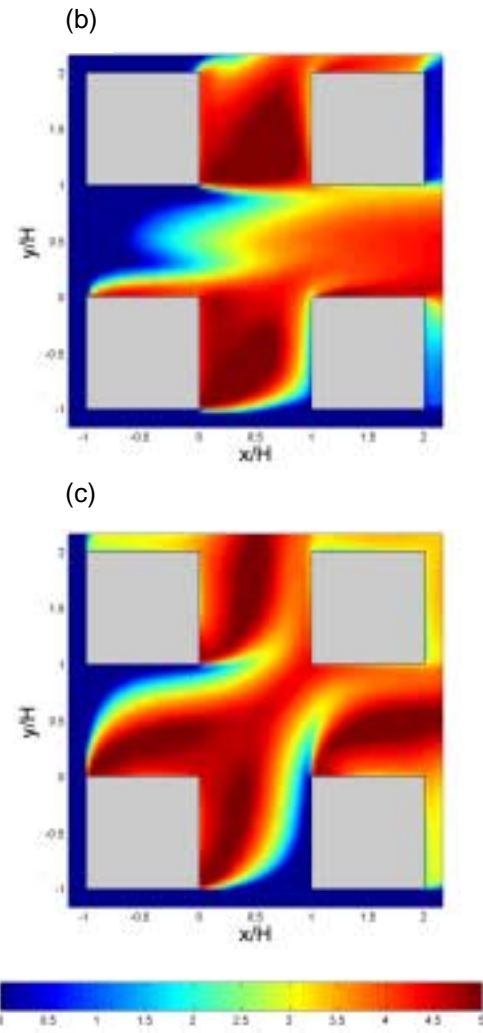
Figure 3. Concentration fields (log scale in base 10) at z/H= 0.17 in the cases of (a) θ = 0°, (b) θ = 15°, and θ = 45°.

(a)